Why the Weather is Unpredictable,
An Experimental and Theoretical Study of the Lorenz Equations

AN HONORS THESIS
PRESENTED TO
THE FACULTY OF THE DEPARTMENT OF MATHEMATICS
AND THE DEPARTMENT OF PHYSICS
BATES COLLEGE

IN PARTIAL FULFILLMENT OF THE REQUIREMENTS FOR THE
DEGREE OF BACHELOR OF SCIENCE

by
Christopher A. Danforth
Lewiston, Maine
March 16, 2001

Acknowledgments

I would like to thank several people who have made this thesis possible. Thanks to Chip Ross for your guidance, patience, and mastery of all things chaotic. I'd be a clueless weatherman if it weren't for you! Thanks to Mark Semon for your technical support and magical proofreading skills. Thanks to George Ruff for your enthusiasm towards physics and life. I wouldn't have majored in physics if it weren't for your influence. Thanks to Molly and Lank for making life fun even when thesis wasn't. Thanks to Fowler, Josh, Kelley, Lindsay, Bouchard, and all of the other physics majors who gave me a crash course in the world of circuits and soldering. Thanks to Laura for making me laugh. Thanks to Mom for making me appreciate the importance of being positive. Finally, thanks to Dad for being so supportive and showing me how rewarding science can be.

Contents

CHAPTER 1

The Nature of Deterministic Systems

In the early 1960's, a meteorologist and mathematician named Edward Lorenz was working on a problem in fluid dynamics. He was trying to create a theoretical model of the atmosphere in order to better understand atmospheric dynamics. As part of his model, Lorenz simplified the usual complicated numerical weather forecasting equations into a set of ordinary differential equations. In this seemingly simple step in the process of mathematical modeling, he stumbled upon a new phenomenon, one which subsequently became known as Chaos.

Lorenz was attempting to find a model in which the usual fluid equations describing the atmosphere were especially simple. He chose as his simplified model a particular set of ODEs which are now referred to as the Lorenz equations, for two reasons. First, the equations for atmospheric dynamics involve thousands of variables and parameters (BUR). Such systems are so complicated that even modern computers can't always use them to make accurate predictions. In Lorenz's time, any attempts to model the atmosphere were painfully slow and revealed little insight into the behavior of the actual weather. Secondly, as Lorenz became more convinced that unpredictability was an inherent part of these deterministic equations, he wanted to show that even a simple set of equations derived from them will have solutions whose behavior is unpredictable (LOR1, 134).

In 1961, when Lorenz was looking for a system to describe the behavior he was interested in, he consulted Barry Saltzman. Saltzman was modeling convective fluid motion and had found a number of periodic solutions to the set of 7 ODEs he was using as his model (LOR3, 137). He complained to Lorenz that while four of the variables inevitably reached a steady state for all initial conditions, there were particular conditions for which the other three variables would not settle down. This nonperiodic behavior inherent in Saltzman's model turned out to be exactly what Lorenz had been searching for: an apparently simple model of atmospheric behavior consisting of coupled differential equations that exhibit nonlinear behavior.

The Lorenz equations were developed from the system of equations used by Saltzman (SLZ) to study the thermodynamic process known as convection. Convection creates the forces that are responsible for the motion of the Earth's atmosphere. Given any fluid, convection will occur when the fluid is heated from below and cooled from above. If a fluid-specific temperature difference between the top and bottom of an "atmosphere" is achieved, the fluid will exhibit cylindrical rolls. Convection occurs everywhere: in the ocean, in the Earth's atmosphere, even in a coffee cup. In the Earth's atmosphere, we consider the air to be a fluid. This fluid is heated by the sun, primarily at the Earth's surface, while being cooled by space and the ocean (LOR2, 403). The complex interactions between these enormous sources and sinks of energy result in the circulation of the atmosphere, as well as in the creation of clouds, storms, and an endless supply of wind, rain, and snow. Modeling the behavior of this system is a difficult task for many reasons.

For centuries, scientists considered the atmosphere as a deterministic system, like a careening billiard ball whose behavior is - at least in principle - predictable. That is to say, people believed that if we knew the equations that govern the atmosphere, and if we knew

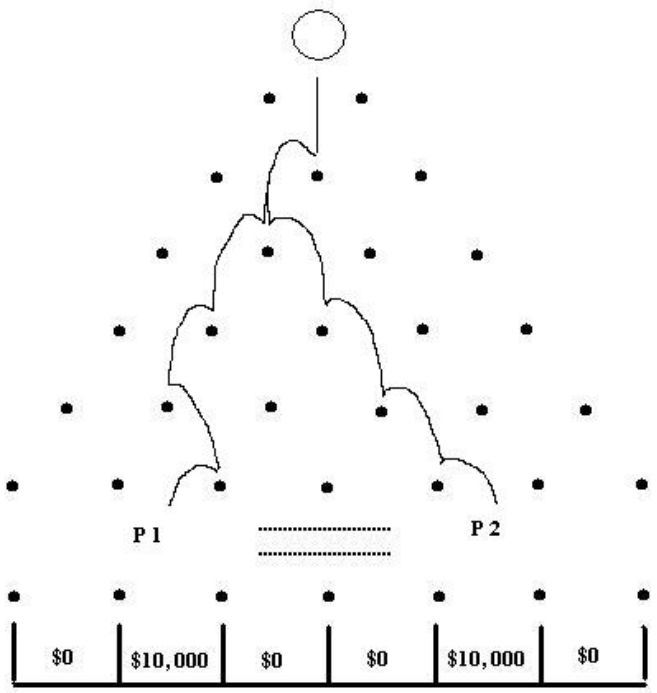

FIGURE 1. Plinko

the exact conditions of the atmosphere at any given time, then we could accurately predict the weather everywhere on Earth, from now until the end of time. Scientists were correct in assuming that the system of equations is deterministic, but they were not prepared for the dramatic impact the initial conditions would have on the predictions made using these differential equations.

Although the equations describing the Earth's atmosphere are equally as deterministic as those of the billiards ball in that the current state of the system determines the next state, they are far more complicated. There are so many variables to consider beyond pressure, humidity, and temperature, that any attempt to produce equations describing the motion of the atmosphere will necessarily involve gross simplifications and therefore cannot completely describe the actual behavior. And while powerful computers are currently capable of forecasting the weather a few days in advance, we still will never make exact predictions about the atmosphere. The reason for this is that we can never know any variable describing a property of the atmosphere to within an arbitrarily small uncertainty. However accurately we measure a variable, our instruments of measurement always will have some inherent uncertainty or margin of error.

Unlike the billiard ball, the Earth's atmosphere exhibits what is called a "sensitive dependence on initial conditions," or SDIC. Systems that are deterministic, but which often appear to be random, are difficult to predict because the uncertainty in measurement will eventually result in a divergence between the system's actual behavior and the model's prediction thereof. "In some dynamical systems it is normal for two almost identical states to be followed, after a sufficient time lapse, by two states bearing no more resemblance than two states chosen at random from a long sequence (LOR3, 8)." A simple example of SDIC is given by the game Plinko, shown in figure 1, which is played on the television game show "The Price is Right." In this game, contestants are given three plinko chips, which are

shaped like hockey pucks. The chips are released adjacent to a vertical wall filled with pegs which are offset from row to row. The pegs are designed to ensure that the plinko chip travels a "random" path before landing at the bottom of the board, where a monetary value is awarded.

Let's assume a contestant on the game show drops her first plinko chip and it travels a path P_1 down the board, landing in the \$10,000 bin. With her second attempt, the contestant might try to drop the plinko chip from the exact same location as the first chip. If she does a good job of recreating the initial conditions of the first drop, the chip will probably bounce in the same direction after the first, second, and maybe even the third peg on the board. But no matter how vigilantly the contestant tries to recreate the chip's motion, the path P_2 of the second chip will almost certainly be different from P_1. For example, if the second chip weighs a fraction of an ounce more than the first, or if the contestant's thumb sticks to the chip for an extra fraction of a second, or if the spin on the chip is slightly different, the two paths can and will diverge from each other. The plinko game is a good example of a system that is deterministic, but whose behavior in practice is unpredictable because of its SDIC. The system is so sensitively dependent upon initial conditions that the tiniest difference between drops will result in totally different trajectories.

Fortunately, there are a number of aspects of chaotic systems which are predictable and orderly. Despite the unpredictability of weather on a daily time scale, seasonal weather patterns are very orderly. Even when extreme weather conditions do arise, the Earth's atmosphere usually returns to more familiar weather patterns. Furthermore, while there are infinitely many possible conditions of the Earth's atmosphere, only a finite number of these states are physically meaningful. For example, the temperature of the water off of the coast of Maine will probably never top 100° F, despite the fact that such a condition is possible. The state of the atmosphere is bounded in a sense by those extreme weather conditions which rarely occur. The conditions towards which the Earth's atmosphere is "attracted" form what is called an attractor. We will discuss the attractor associated with Lorenz's convection model later in this thesis.

Even simple systems like plinko can exhibit chaotic behavior, making predictions difficult. But by reducing complicated systems into simple ones through modeling, we can learn more about the different consequences resulting from the SDIC in each case. We now examine a relatively simple mathematical model of the atmosphere, and then describe an experiment based upon it that can be used to illustrate some surprising effects that result from the system's SDIC.

CHAPTER 2

The Lorenz Equations

Much of the emphasis on the Lorenz equations, in both differential equations textbooks and in the popular literature, is on the dynamics of the Lorenz system. Indeed, the Lorenz attractor and other properties of chaos predicted by the Lorenz equations are enough to fill an entire textbook. On the other hand, the derivation of the Lorenz equations is almost always left as an exercise for the intrigued and mathematically experienced reader. Therefore, the mathematical development of the Lorenz equations from the equations of momentum and fluid flow is the subject of this chapter.

Temperature Deviation

As mentioned in Chapter 1, the Lorenz model is used to describe convective motion in a fluid. The fluid is contained in a long, thin cell, bounded above and below by parallel plates. The top plate maintains a temperature T_c, while the bottom plate is held at a temperature T_w, where $T_w > T_c$. The temperature difference $\Delta T = T_w$ - T_c is fixed, but can be adjusted to create different types of behavior. The system is given by the fluid contained in the cell, heated from below by the hot plate and cooled from above by the cold plate. It was first studied experimentally by Bénard in 1900, and then theoretically by Lord Rayleigh in 1916 (HLB, 29). As a result, this configuration is called a Rayleigh-Bénard cell.

The convection cell is used to simulate the qualitative behavior of the atmosphere. The sun heats the Earth's atmosphere and surface, providing an enormous source of thermal energy. The ocean and space siphon that energy out of the atmosphere. As this "tug of war" takes place, the air above the warm ground rises due to convection until it reaches the dew point where it condenses to form clouds. On the other hand, as the outermost layer of the atmosphere is cooled by space, it becomes more dense and falls. In this way convection currents are created in the atmosphere, and we have weather (BUR, 12).

In a convection cell, if ΔT remains small, the fluid remains still, and the heat energy released by the bottom plate is absorbed by the pockets of fluid in the bottom of the cell. This heat is then transfered to the top of the fluid through thermal conduction. The density of a small pocket of fluid decreases as the fluid is heated, so a pocket near the bottom plate experiences a buoyancy force pushing upward. However, when the cell is in a conductive state, the pocket of fluid loses heat to neighboring cool pockets before it has time to rise in the cell. In such a situation, the temperature in the cell falls linearly with vertical position from T_w at the bottom of the cell to T_c at the top (HLB, 29), see figure 2.

The temperature T_d at any location (x, z, t) in the cell while the fluid is in a conductive state, where no motion is present, can thus be described

$$T_d(x, z, t) = T_w - \frac{z}{h}\Delta T, \tag{1}$$

where z is the vertical height in the cell measured from the bottom, x is the horizontal position, and h, the height of the cell, is fixed. Because the cell is thin, the motion is essentially two dimensional, so there is no depth component in any of the functions concerning

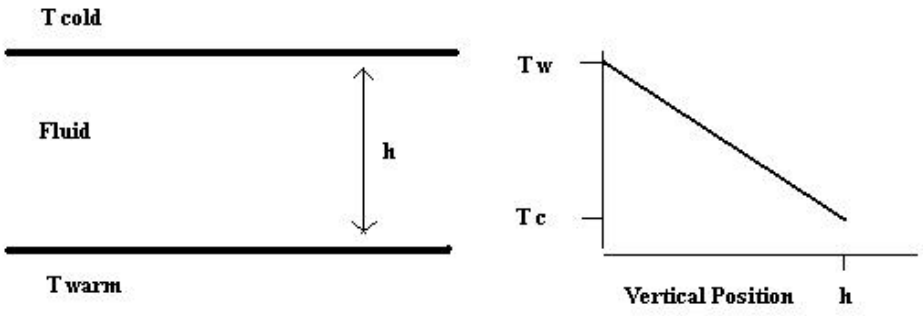

FIGURE 2. Conduction in a Rayleigh-Bénard cell

the fluid flow. The temperature is assumed constant for all y values, or depths, of the cell. As we would expect, the boundary conditions ensure that at height $z = 0$ in the cell, $T_d(x, 0, t) = T_w$ for all values of x and t. At a height $z = h$, $T_d(x, h, t) = T_c$. Finally, in the center of the cell at $z = h/2$, the linear function $T_d(x, h/2, t)$ gives us the average temperature between the top and bottom plates.

When the temperature difference ΔT grows past a threshold value, the buoyancy force on the pocket of fluid overcomes the viscous force and gravity, and the fluid pocket begins to rise before it loses an appreciable amount of heat energy through conduction. Once the fluid has risen into a region of lower temperature and higher density, the buoyancy force increases, because the pocket is less dense than its neighbors (HLB, 605). If the upward force is strong enough, the pocket of warm fluid will continue to move up faster than it can cool off. Rising pockets of warm fluid push their way to the top of the cell, displacing the cooler pockets of fluid. These cooler pockets are more dense, and are pushed down towards the bottom of the cell. The process repeats itself causing convection rolls to appear in the cell, and the cell is thus in a convective state, see figure 3.

Let $T_v(x, z, t)$ be the temperature of the fluid at a point (x, z) at time t, when it's in a convective state. We next define a function that measures the deviation of the convective state temperature T_v from the conductive state temperature T_d. This deviation function is defined as

$$\varphi(\mathrm{x,z,t}) = T_v(x, z, t) - T_d(x, z, t), \tag{2}$$

and can be written as

$$\varphi(\mathrm{x,z,t}) = T_v(x, z, t) - T_w + \frac{z}{h}\Delta T. \tag{3}$$

Since the temperatures of the top and bottom plates are fixed, we expect that when $z = 0$ and $z = h$, the convective state temperature $T_v(x, z, t)$ will agree with the conductive temperature function $T_d(x, z, t)$, and the deviation will be 0, ie. $\varphi(x, 0, t) = 0$ and $\varphi(x, h, t) = 0$ for all x and t. Notice that this means the temperature of the fluid at the very top and bottom of the cell is the same for both convection and conduction.

Navier-Stokes and Thermal Energy Equations

We now describe the relationship between the motion of a heated fluid and the forces associated with heating. The Navier-Stokes equations for fluid flow are often used to obtain

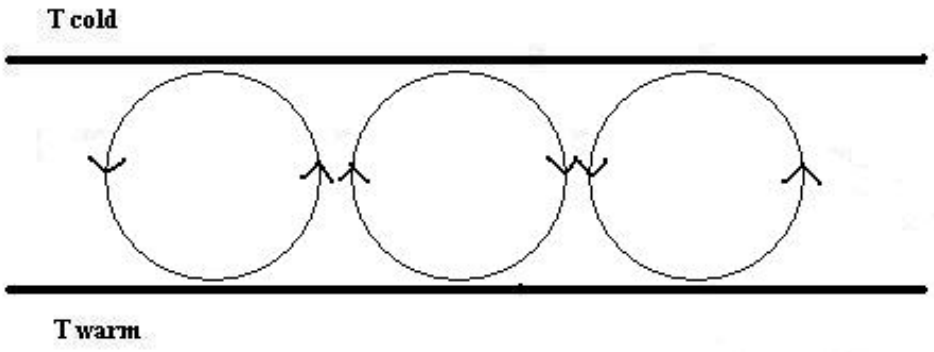

FIGURE 3. Convection cells

a quantitative description of fluid dynamics. Once again, convective motion is taken to be independent of depth y in the cell, so only the horizontal and vertical components of the fluid velocity $\vec{v}$ are of interest. The two equations for conservation of momentum in a fluid are

$$\rho\frac{\partial v_z}{\partial t} + \rho\vec{v}\cdot\nabla v_z = -\rho g - \frac{\partial p}{\partial z} + \mu\nabla^2 v_z \tag{4}$$
$$\rho\frac{\partial v_x}{\partial t} + \rho\vec{v}\cdot\nabla v_x = -\frac{\partial p}{\partial x} + \mu\nabla^2 v_x$$

In these fluid transport equations, ρ is the mass density of the fluid and is a function of temperature, g is the acceleration due to gravity, p is the fluid pressure and is a function only of the height z, and μ is the fluid viscosity (HLB, 608). The vector representing the fluid flow velocity, $\vec{v}$, is composed of velocity components v_x and v_z which are each functions of x, z, and t. The first term on the left side of equation (4) accounts for the fact that the momentum of a pocket of fluid will change as the pocket accelerates. The second term shows how momentum changes as the pocket of fluid moves to an region where the momentum is different. This advection term is nonlinear in the velocity, and accounts for the chaotic behavior of the system. The right side of equation (4) represents the sum of the forces acting on a small pocket of fluid. The three forces involved are gravity, fluid pressure, and viscosity. As one would expect, gravity has no effect on the x component of the fluid velocity.

The temperature of the fluid can be described by the thermal energy diffusion equation, satisfied by our convective temperature function T_v as follows

$$\frac{\partial T_v}{\partial t} + \vec{v}\cdot\nabla\ T_v = D_T\nabla^2 T_v, \tag{5}$$

where D_T represents the thermal diffusion coefficient. This coefficient depends on the type of fluid and the viscosity of the fluid. If D_T is large, then the fluid molecules will spread out quickly as a result of heating (HLB, 509). The thermal diffusion equation gives us information about how heat energy is dispersed by a pocket of fluid, and in which direction. In order to find the thermal energy diffusion equation in terms of our temperature deviation function φ, we substitute T_v from equation (3) into (5), resulting in

$$\frac{\partial(\varphi + T_d)}{\partial t} + \vec{v}\cdot\nabla\ (\varphi + T_d) = D_T\nabla^2(\varphi + T_d). \tag{6}$$

Since T_d is independent of x and t, (6) reduces to

$$\frac{\partial \varphi}{\partial t} + \vec{v} \cdot \nabla \ \varphi - \vec{v_z} \frac{\Delta T}{h} = D_T \nabla^2 \varphi. \tag{7}$$

The mass density of the fluid, ρ, decreases as the fluid is heated and increases when the fluid is cooled. As a result, ρ is a function of the temperature T_v, which we will write in terms of a power series expansion

$$\rho(T_v) = \rho_o + \frac{d\rho}{dT}\Big|_{T_w} (T_v - T_w) + ... \tag{8}$$

where $\rho_o = \rho(T_w)$. If we then define the thermal expansion coefficient α by

$$\alpha = -\frac{1}{\rho_o} \frac{d\rho}{dT}\Big|_{T_w}, \tag{9}$$

and substitute our temperature deviation function into the power series for ρ, the first two terms become

$$\rho(T_v) = \rho_o - \alpha \rho_o [\varphi(x, z, t) - \frac{z}{h} \Delta T]. \tag{10}$$

Only the first two terms in the power series for $\rho(T_v)$ are shown in (10) because of the small variation in density throughout the fluid cell. This simplification, known as the Boussinesq Approximation, is valid for systems in which the variation in density is due only to small variations in temperature (CHN, 16). In other words, when the temperature variations throughout the cell are small, there is a negligible difference in volume expansion, on the order of 10^{-4}. As a result, we can ignore all but the linear terms in the power series for $\rho(T_v)$.

In the Navier-Stokes equations (4), the Boussinesq Approximation further reduces the density variation by allowing us to substitute $\rho(T_v) = \rho_o$ into all of the terms except the one involving gravity (CHN, 16). For the term involving gravity, we insert the linear approximation of $\rho(T_v)$. The fluid pressure function p is then replaced by an effective pressure gradient function β which has the condition that β is a constant when the fluid is in a conducting state (HLB, 609). In a convecting state, the pressure gradient is

$$\beta = p + \rho_o g z + \alpha \rho_o g \frac{z^2}{2} \frac{\Delta T}{h}. \tag{11}$$

When we substitute the pressure gradient β into the Navier-Stokes equations, use the Boussinesq Approximation twice, and divide by ρ_o, we arrive at

$$\begin{aligned} \frac{\partial v_z}{\partial t} + \vec{v} \cdot \nabla v_z &= -\frac{1}{\rho_o} \frac{\partial \beta}{\partial z} + \alpha \varphi g + \nu \nabla^2 v_z \\ \frac{\partial v_x}{\partial t} + \vec{v} \cdot \nabla v_x &= -\frac{1}{\rho_o} \frac{\partial \beta}{\partial x} + \nu \nabla^2 v_x \end{aligned} \tag{12}$$

where $\nu = \mu / \rho_o$ is the kinematic viscosity, around $1.1 * 10^{-5}\ m^2/s$ for water (PAT, 133).

Now that we have a form of the Navier-Stokes equations more specific to our two dimensional cell, we need make only a few more transformations before we can attempt to find a solution. It will be more convenient when trying to understand the effect each parameter has on the system if all of the variables are in a unitless form. To do this, we first define a new time parameter t' as

$$t' = \frac{D_T}{h^2} t, \tag{13}$$

where h^2 / D_T is a typical time for thermal energy to diffuse over a distance h (HLB, 610). The unitless distance variables are defined as $x' = x/h$ and $z' = z/h$. The unitless temperature

variable is defined as $\varphi' = \varphi/\Delta T$. Based on these variables, the unitless velocity can then be defined as

$$v_x{}' = \frac{D_T}{h} v_x \tag{14}$$
$$v_z{}' = \frac{D_T}{h} v_z$$

and the time independent, dimensionless Laplacian operator is then defined as $\nabla'^2 = h^2\nabla^2$.

Using these new unitless variables and multiplying by a constant, we can rewrite the Navier-Stokes equations (12) without the primes as follows

$$\frac{D_T}{\nu}[\frac{\partial v_z}{\partial t} + \vec{v}\cdot\nabla v_z] = -\frac{h^2}{\nu D_T \rho_o}\frac{\partial p}{\partial z} + \frac{\alpha \Delta T g}{\nu D_T} h^3\varphi + \nabla^2 v_z \tag{15}$$
$$\frac{D_T}{\nu}[\frac{\partial v_x}{\partial t} + \vec{v}\cdot\nabla v_x] = -\frac{h^2}{\nu D_T \rho_o}\frac{\partial p}{\partial x} + \nabla^2 v_x$$

Many significant ratios of parameters appear in the unitless form of the Navier-Stokes equations. As a result, some of them have been given names. The Rayleigh number R is an important parameter describing the balance between the buoyancy force on a pocket of fluid as a result of thermal expansion with the loss of energy to thermal diffusion and viscosity (HLB, 611). It is a unitless parameter that can be adjusted by changing the temperature difference ΔT, and is important in determining the value of ΔT at which convection will begin. It is defined as

$$R = \Delta T \frac{\alpha g h^3}{\nu D_T}. \tag{16}$$

The Rayleigh number is the most important parameter of a fluid flow system and will be discussed in more detail later. The second ratio is the Prandtl number σ which gives the ratio of kinematic viscosity to the thermal diffusion coefficient (HLB, 611),

$$\sigma = \frac{\nu}{D_T}. \tag{17}$$

The Prandtl number compares the amount of energy lost to shearing of the fluid in motion with the energy lost to conductive heat flow in the fluid (HLB, 611). If the Prandtl number is greater than 1, the fluid loses more mechanical energy in motion than it does to heat flow. For example, water at room temperature has $\sigma \approx 7$. Both the Rayleigh number, R, and the Prandtl number, σ, are important parameters in the Lorenz system. Small adjustments in these parameters can turn a stable or periodic fluid flow into one which is turbulent or chaotic (GSN). The exact requirements of unstable flow will be discussed later.

The final dimensionless ratio Π is related to the pressure of the fluid and is defined to be

$$\Pi = \frac{\beta h^2}{\nu \rho_o D_T}. \tag{18}$$

Using the unitless variables and the three ratios defined above, we can rewrite the Navier-Stokes equations (15) as

$$\frac{1}{\sigma}[\frac{\partial v_z}{\partial t} + \vec{v}\cdot\nabla v_z] = -\frac{\partial \Pi}{\partial z} + R\varphi + \nabla^2 v_z \tag{19}$$
$$\frac{1}{\sigma}[\frac{\partial v_x}{\partial t} + \vec{v}\cdot\nabla v_x] = -\frac{\partial \Pi}{\partial x} + \nabla^2 v_x$$

Making the same substitutions, the thermal energy diffusion equation (7) becomes

$$\frac{\partial \varphi}{\partial t} + \vec{v}\cdot\nabla\varphi - v_z = \nabla^2\varphi. \tag{20}$$

It should be noted that by grouping together constants and functions into the parameters R, σ, and Π, we have *not* introduced any further simplifications to our model of convection. We are merely gathering together variables to create parameters with physical meaning. Equations (19) and (20) will be used to find a fluid streamfunction that describes the motion of the fluid.

Fluid Streamfunction

The vector representing the fluid flow velocity, $\vec{v} = \vec{v}(x, z, t)$, which appears in equations (19) and (20), can always be deduced from a fluid streamfunction $\Psi(x, z, t)$. The streamfunction supplies all of the important information about the fluid flow. At any time t, the function $\Psi(x, z, t)$ provides the streamlines of the fluid motion (HLB, 493). The fluid velocity vector $\vec{v}$ is tangent to a streamline, with Ψ defined such that its gradient is perpendicular to $\vec{v}$ according to the relations

$$v_x = -\frac{\partial \Psi(x,z,t)}{\partial z} \tag{21}$$
$$v_z = \frac{\partial \Psi(x,z,t)}{\partial x}$$

The negative sign could be placed in front of either velocity component, but this choice results in the conventional Lorenz equations (HLB, 612). When we expand the gradient and dot product in equation (20), we get

$$\vec{v} \cdot \nabla \varphi = -\frac{\partial \Psi}{\partial z}\frac{\partial \varphi}{\partial x} + \frac{\partial \Psi}{\partial x}\frac{\partial \varphi}{\partial z}. \tag{22}$$

Inserting this term into (20), we find

$$\frac{\partial \varphi}{\partial t} - \frac{\partial \Psi}{\partial z}\frac{\partial \varphi}{\partial x} + \frac{\partial \Psi}{\partial x}\frac{\partial \varphi}{\partial z} - \frac{\partial \Psi}{\partial x} = \nabla^2 \varphi. \tag{23}$$

This equation is the first differential equation relating the streamfunction Ψ to the temperature difference function φ. The second differential equation is obtained by substituting the velocity components v_x and v_z into equation (19). The v_x equation becomes

$$\frac{1}{\sigma}\left[-\frac{\partial^2 \Psi}{\partial t \partial z} + \frac{\partial \Psi}{\partial z}\frac{\partial^2 \Psi}{\partial x \partial z} - \frac{\partial \Psi}{\partial x}\frac{\partial^2 \Psi}{\partial z \partial x}\right] = -\frac{\partial \Pi}{\partial x} - \nabla^2 \frac{\partial \Psi}{\partial z}, \tag{24}$$

and the v_z equation becomes

$$\frac{1}{\sigma}\left[\frac{\partial^2 \Psi}{\partial t \partial x} - \frac{\partial \Psi}{\partial z}\frac{\partial^2 \Psi}{\partial x^2} + \frac{\partial \Psi}{\partial x}\frac{\partial^2 \Psi}{\partial z \partial x}\right] = -\frac{\partial \Pi}{\partial z} + R\varphi + \nabla^2 \frac{\partial \Psi}{\partial x}. \tag{25}$$

To eliminate the pressure related parameter Π, we take the partial derivative of (25) with respect to x and subtract the partial derivative of (24) with respect to z. The result is

$$\frac{1}{\sigma}\left[\frac{\partial}{\partial t}(\nabla^2 \Psi) - \frac{\partial}{\partial z}\left(\frac{\partial \Psi}{\partial z}\frac{\partial^2 \Psi}{\partial x \partial z} - \frac{\partial \Psi}{\partial x}\frac{\partial^2 \Psi}{\partial z^2}\right) - \frac{\partial}{\partial x}\left(\frac{\partial \Psi}{\partial z}\frac{\partial^2 \Psi}{\partial x^2} - \frac{\partial \Psi}{\partial x}\frac{\partial^2 \Psi}{\partial x \partial z}\right)\right] = R\frac{\partial \varphi}{\partial x} + \nabla^4 \Psi. \tag{26}$$

Equations (23) and (26) describe the motion and temperature of a fluid being heated. They couple the behavior of our functions $\Psi(x, z, t)$ and $\varphi(x, z, t)$.

Truncation and Numerical Analysis

We will now find functions Ψ and φ that satisfy our set of differential equations, along with the appropriate boundary conditions. The boundary conditions for φ were discussed previously, after we defined φ in equation (3). The boundary conditions for Ψ will be satisfied if the partial derivatives in equation (21) satisfy the requirements of convection. We would expect the vertical component of the velocity v_z to be zero at the top, $z = 1$, and bottom, $z = 0$, of the cell. Similarly, the horizontal component of the velocity v_x should be zero at the sides of the cell.

One common technique for finding solutions to a differential equation is to first find a solution that is separable. A separable solution in this case is a function that is the product of three component functions, one for each variable x, z, and t. Consider a solution of the form

$$\Psi(x,z,t) = \sum_{m,n} e^{\omega_{m,n}t}[A_m\cos(\lambda_m z) + B_m\sin(\lambda_m z)] \cdot [C_n\cos(\lambda_n x) + D_n\sin(\lambda_n x)] \tag{27}$$

where each λ is the wavelength of a Fourier spatial mode. The spatial modes depend on the dimensions of the convection cell and are chosen to ensure that the solution satisfies the boundary conditions. Each λ has a corresponding frequency $\omega_{m,n}$ which determines how often the magnitude of the function oscillates (HLB, 614).

Equation (27) is an infinite sum of sine and cosine terms. To make the general solution simpler, the sum is truncated using a process called the *Galerkin procedure* (HLB, 614). We might be concerned that in approximating the equations for Ψ and φ we will lose much of the important nonlinear nature of the system. Fortunately, Saltzman has shown numerically that this truncation still captures most of the important nonlinear behavior (SLZ). Using the Galerkin procedure, we choose a finite number of sine and cosine terms from the Fourier expansion of Ψ. A similar Fourier expansion and Galerkin truncation also results in a general solution for φ. The resulting sum of the truncated equations for the fluid streamfunction and temperature deviation function are

$$\Psi(x,z,t) = \psi(t)\sin(\pi z)\sin(ax) \tag{28}$$

$$\varphi(x,z,t) = T_1(t)\sin(\pi z)\cos(ax) - T_2(t)\sin(2\pi z), \tag{29}$$

where the height of the cell is taken to be 1 so that $z \in$[0,1]. The parameter a is chosen so that the Rayleigh number is at its minimum when convection begins, and will be discussed in more detail later.

The time dependency of $\Psi(x,z,t)$ and $\varphi(x,z,t)$ is represented by $\psi(t)$, $T_1(t)$, and $T_2(t)$ which are unknown functions whose roles in the streamfunction and temperature deviation function we will now discuss. The T_1 term in the temperature deviation function gives the temperature difference between the upward and downward currents in the convection cell. The T_2 term gives the deviation from the linear temperature variation in the center of the cell as a function of z (HLB, 615). Without the T_2 term, the temperature deviation function would not capture the effect of circulation on the diffusion of heat energy.

To see how well the solutions given by (28) and (29) describe convection in a Rayleigh-Bénard cell, we will check the boundary conditions. For the streamfunction, we must see that the vertical component of the velocity, v_z, is zero at the top and bottom of the cell. Similarly, the horizontal component of the velocity, v_x, should be zero at the sides of the

cell. These boundary conditions are easily checked

$$v_z(x,1,t) = \frac{\partial\Psi(x,1,t)}{\partial x} = a\psi(t)\sin(\pi)\cos(ax) = 0 \tag{30}$$
$$v_x(\frac{\pi}{a},z,t) = -\frac{\partial\Psi(\frac{\pi}{a},z,t)}{\partial z} = -\pi\psi(t)\cos(\pi z)\sin(\pi) = 0$$

For the temperature deviation function, we would expect from equation (3) that the deviation at the top and bottom of the cell is zero. This is easily checked in a manner similar to that above. Along the $z = 1/2$ horizontal axis, where $0 < x < \pi/a$, the $T_2(t)$ term vanishes and we are left with $\varphi = T_1(t)\cos(ax)$. The temperature deviation is maximized at (0, 1/2, t) where φ is reduced to $\varphi(t) = T_1(t)$. This position will be known as 9 o'clock in a single convection cell. Likewise, the temperature deviation is most negative at $(\pi/a, 1/2, t)$ or 3 o'clock, where $\varphi(t) = -T_1(t)$. In the very center of a convection cell, at $(\pi/2a, 1/2, t)$, the temperature deviation from linear is 0.

Along the $x = \pi/2a$ axis, the $T_1(t)$ term disappears and we are left with $\varphi(t) = -T_2(t)\sin(2\pi z)$. Then for $0 < z < 1/2$, $\varphi(t) = -T_2(t)N$ where both N and T_2 are positive. This implies that any pocket of fluid below $z = 1/2$ on the $x = \pi/2a$ axis is cooler than predicted by a linear temperature variation. Likewise, for $1/2 < z < 1$, $\varphi(t) = T_2(t)N$. This implies that a pocket of fluid above $z = 1/2$ on the same axis is warmer than it should be. Both these implications are consistent with our understanding of how a pocket of fluid will move when it exhibits convection rolls. A warm pocket of fluid below $z = 1/2$ will rise in the cell, displacing a cold pocket somewhere above $z = 1/2$. Once the warm pocket reaches the upper half of the cell, it is warmer than predicted by the linear temperature function associated with conduction (1). Consequently, φ will return a positive number, indicating that the convecting pocket of fluid is warmer than a conducting pocket would be.

Lorenz Equations

To obtain the final form of the Lorenz equations, we substitute our expressions for Ψ, (28), and φ, (29) into the differential equations (23) and (26). The result is simplified by the following relations for the time independent Laplacian operator

$$\nabla^2\Psi = -(\pi^2 + a^2)\Psi \tag{31}$$
$$\nabla^4\Psi = (\pi^2 + a^2)^2\Psi$$

Inserting the solution functions (28) and (29) into equation (26) gives

$$\frac{-d\psi(t)}{dt}(\pi^2 + a^2)\sin(\pi z)\sin(ax) = -\sigma R T_1(t)\sin(\pi z)\sin(ax) \tag{32}$$
$$+ \sigma(\pi^2 + a^2)^2\psi(t)\sin(\pi z)\sin(ax).$$

When we equate the coefficients of the $\sin(\pi z)\sin(ax)$ terms, the result is

$$\frac{d\psi(t)}{dt} = \frac{\sigma R}{\pi^2 + a^2}T_1(t) - \sigma(\pi^2 + a^2)\psi(t). \tag{33}$$

When we substitute the proposed solution functions Ψ and φ into equation (23), we find

$$\begin{aligned}(34)\quad \frac{dT_1}{dt}\sin(\pi z)\cos(ax) - \frac{dT_2}{dt}\sin(2\pi z) + (\pi^2+a^2)^2 T_1 \sin(\pi z)\cos(ax) \\ - 4\pi^2 T_2 \sin(2\pi z) - \psi a \sin(\pi z)\cos(ax) \\ = -[\psi\pi\cos(\pi z)\sin(ax)][T_1 a\sin(\pi z)\sin(ax)] \\ - [\psi a\sin(\pi z)\cos(ax)][T_1\pi\cos(\pi z)\cos(ax)] \\ + [\psi\sin(\pi z)\cos(ax)][2\pi T_2\cos(\pi z)\cos(ax)].\end{aligned}$$

Many of the terms in equation (34) have $\sin(\pi z)\cos(ax)$ in them. If we equate these terms, dropping one term whose spatial dependence is beyond the scope of our model (HLB, 616), we are left with

$$(35)\qquad \frac{dT_1(t)}{dt} = a\psi(t) - (\pi^2+a^2)T_1(t) - \pi a\psi(t)T_2(t).$$

The other terms in the temperature deviation equation (34) are multiplied by $\sin(2\pi z)$. Equating these terms we have

$$(36)\qquad \frac{dT_2(t)}{dt} = \frac{\pi a}{2}\psi(t)T_1(t) - 4\pi^2 T_2(t).$$

These three equations, (33),(35), and (36), relate the time dependent part of the stream-function, ψ(t), to the temperature gradient functions T_1(t) and T_2(t). They are the three differential equations describing all motion in the Lorenz system. To obtain the final form of the Lorenz equations, we make a few more substitutions. We introduce the new time variable

$$(37)\qquad t' = (\pi^2+a^2)t,$$

and the reduced Rayleigh number r

$$(38)\qquad r = \frac{a^2}{(\pi^2+a^2)^3}R.$$

The reduced Rayleigh number is defined so that when $r \leq 1$, the fluid is in a conductive or stable state. So for our discussion, $r > 1$ implies that the fluid will start rolling. This means

$$(39)\qquad R \geq \frac{(\pi^2+a^2)^3}{a^2}$$

is the condition necessary for convection.

The parameter a is related to the width of the convection cell in the x-direction. We choose $a = \pi/\sqrt{2}$, so that R is as small as possible while still satisfying Equation (39). Physically, this means that for a cell with height 1, convection rolls will begin to appear when the horizontal width of the cell is chosen to be greater than or equal to $\sqrt{2}$. Any smaller value for a would restrict the fluid in the cell from exhibiting convection rolls. Any larger value for a would merely complicate our model. This choice for a gives the Rayleigh number at which convection begins, $R = 27\pi^4/4$ (HLB, 618).

Finally, the parameter b is defined as

$$(40)\qquad b = \frac{4\pi^2}{\pi^2+a^2},$$

where the condition for convection, $a = \pi/\sqrt{2}$, gives us a value of $b = 8/3$.

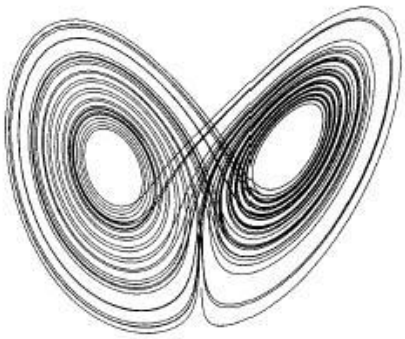

FIGURE 4. Lorenz Attractor

We will also rename ψ, T_1, and T_2 with the new time variable as follows

$$X(t) = \frac{a\pi}{(\pi^2 + a^2)\sqrt{2}}\psi(t) \tag{41}$$
$$Y(t) = \frac{r\pi}{\sqrt{2}}T_1(t)$$
$$Z(t) = r\pi T_2(t)$$

Taking these definitions for X, Y, and Z, and substituting them into equations (33), (35), and (36), we arrive at the final form of the Lorenz equations

$$\frac{dX}{dt} = \sigma Y(t) - \sigma X(t) \tag{42}$$
$$\frac{dY}{dt} = rX(t) - X(t)Z(t) - Y(t)$$
$$\frac{dZ}{dt} = X(t)Y(t) - bZ(t)$$

These equations are used to study one of the most mathematically complicated objects ever discovered, the Lorenz attractor. The Lorenz attractor, often called the "butterfly" attractor because of its wings, is the shape associated with every initial condition of the Lorenz equations. The trajectory never intersects itself, despite coming arbitrarily close. An example of the Lorenz attractor is shown in figure 4. The solution curve for the initial condition (0, 9, 3) is traced out by the Lorenz equations in three dimensional phase space. The behavior of the trajectory is far more interesting when viewed in real time while the attractor is being drawn. The solution loops around two foci, located at ($6\sqrt{2}$, $6\sqrt{2}$, 27) and (-$6\sqrt{2}$, -$6\sqrt{2}$, 27), like a planet orbiting two suns. The "gravitational" pull of one focus will only dominate the trajectory for a short time before it is tugged away by the pull of the other.

As we shall see, the behavior of the solutions to this set of coupled differential equations is extremely complicated and beautiful. However, their development is very rarely mentioned in any of the mathematics texts which discuss the Lorenz system. This could be a result of the difficulty mathematicians have in justifying the approximations and truncations required by the derivation. Fortunately, Lorenz wasn't looking for an exact description of the fluid flow in Rayleigh-Bénard convection. He was merely trying to find a simple system of equations to illustrate numerical weather forecasting. In developing the equations, he "proceeded in the manner of a professional meteorologist and an amateur mathematician"

(LOR3, 132). If he hadn't made so many approximations in his paper *Deterministic Nonperiodic Flow* (LOR1), Lorenz may never have discovered this system. Unfortunately for the general scientific community, he published in the Journal of the Atmospheric Sciences. As a result, it took almost a decade for the physics and mathematics communities to realize what he had discovered.

CHAPTER 3

A Simple Model of the Weather

Very few attempts have been made to design an experimental apparatus demonstrating the type of behavior predicted by the Lorenz equations. This is surprising considering how important the effects of Lorenz type chaos might be in weather prediction. By studying the dynamics of the Lorenz equations in an actual convection experiment, we expect to acquire more insight into the type of phenomena they predict, and some insight into how they might be used to improve our ability to forecast the weather.

Thermosyphon

One simple model of convection in the Earth's atmosphere is the thermal convection loop, or thermosyphon. The thermal convection loop is a torus shaped tube, filled with fluid, standing in the vertical plane. The bottom half of the tube is heated at a constant rate while the top half is cooled at a constant rate. The circular geometry of the thermosyphon is chosen in order to force the fluid to exhibit mathematically convenient circular convection rolls. Thermocouples are inserted into the tube at 3, 6, and 9 o'clock on the face of the loop to measure the temperature of the fluid at each position (labeled B, C, and A respectively in Figure 5).

The thermocouples are inserted as close to the center of the tube as possible to avoid misleading readings, since the behavior of the fluid is not uniform across the entire diameter of the tube. Furthermore, by taking measurements of the temperature near the center, we avoid complications which arise near the boundary.

The temperature sensor at point C is used to find the average temperature of the fluid in the bottom half of the tube at any given time. The sensors at points A and B are used to establish the temperature difference during convection between the warm, rising fluid and the cool, falling fluid. The temperatures at points A and B will be labeled T_A and T_B. The difference between the temperatures at these two points is an important quantity, and is defined to be

$$\delta \mathrm{T} = T_A \text{ - } T_B. \tag{43}$$

The temperature at point C will be called T_w, corresponding to the temperature of the lower plate in the Rayleigh-Bénard convection cell model.

The fluid in the thermosyphon is initially at rest, with the heat energy from the bottom half of the tube being transfered to the top half by conduction. The fluid in the tube will begin to rotate when the temperature difference between the top and bottom halves of the loop is great enough to create the density variation required for buoyancy to overcome gravity and viscosity (HLB, 605). Fluid in the top half of the loop is cooled, making it heavier and more likely to sink. Fluid in the bottom half of the loop is heated, making it less dense and more likely to rise. Consequently, the fluid will eventually begin to circulate around the tube.

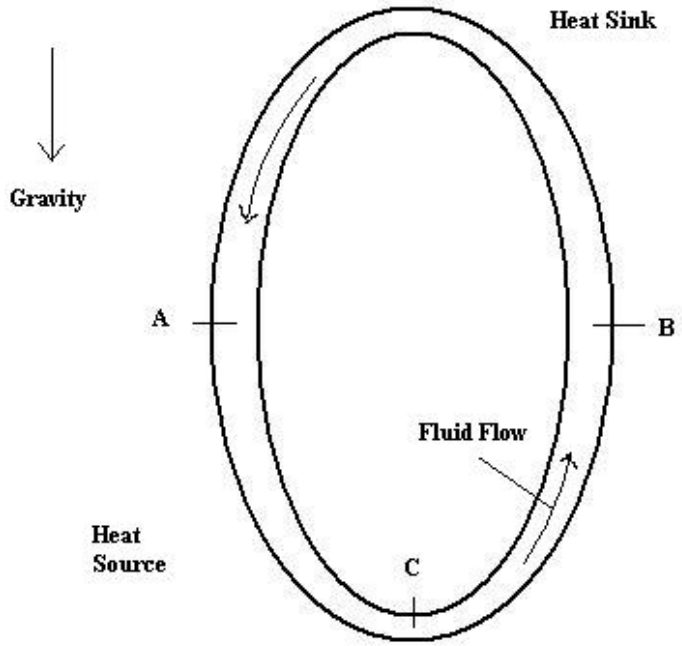

FIGURE 5. Thermal Convection Loop

When the heating and cooling rates are held constant, an initially stationary fluid will accelerate until the effects of buoyancy and friction balance each other out (CRV, 65). Once an equilibrium is achieved, the fluid flow rate should be constant in both magnitude and direction, a steady state. However, under certain conditions, a steady state is never reached by the fluid in a thermal convection loop. When the temperature difference between the top and bottom halves of the loop is within a particular range, the fluid oscillates in an unstable and chaotic manner. The stable and unstable states of fluid oscillation in a thermal convection loop are the topic of this chapter.

Theory

The theoretical predictions that have been made concerning thermosyphons are all dependent upon the heating and cooling rates used to force convection in the fluid. Our experimental apparatus uses the air at room temperature to cool the fluid rather than a coolant filled sleeve. The resulting behavior is the same as long as a large enough δT is created. Consequently, we will only discuss the theoretical predictions regarding the heating rate, since the cooling rate is relatively constant.

At the beginning of each trial, a heating rate V is chosen to heat the bottom half of the tube. This rate remains unchanged throughout each experimental trial. When the heat source is switched on to supply V, the heat energy initially conducts up through the fluid from the bottom of the tube to the top. Small pockets of fluid lose heat to neighboring pockets before they have time to rise. During this initial conduction stage, the temperature throughout the entire tube rises slowly. This conduction stage continues until the threshold

temperature for convection is reached. For any heating rate $V < V_i$, the threshold temperature is never reached. The heating rate V is not strong enough to force the fluid to convect, so the fluid remains motionless. Conduction slowly warms up the fluid throughout the tube, but no rotational motion occurs.

For heating rates of $V > V_i$, the initial conducting state of the fluid changes to a convecting state within minutes. The direction in which the fluid begins rotating is determined, but in reality it is impossible to predict, much like the flip of a coin. In a stable state of the convection cell, once the fluid has chosen a direction in which to rotate, be it clockwise or counterclockwise, that direction will remain unchanged as long as the conditions under which it was produced are unchanged.

The onset of convection can be observed by watching the temperature difference δT described in equation (43). If $|\delta T| > 0$, the temperature is greater on one side of the tube than the other, and the fluid has begun to rotate. For example, if δT = T_A - T_B is less than zero, then we know the temperature of the water is greater at point B than at point A and the fluid must be rotating in a counterclockwise direction. The logic behind this assertion is as follows.

Assume the water in the tube has begun to rotate in a counterclockwise direction, as in figure 5. A pocket of fluid beginning near point A on the loop at time t_1 is constantly heated as it travels around the bottom half of the loop, past point C. By the time the pocket of fluid reaches point B, it has experienced the maximum amount of heating that the heat source has to offer. At that moment, time t_2, it is the hottest pocket in the entire tube. Now imagine the pocket of fluid which begins just above point B at time t_1, antipodal to the pocket just discussed. This pocket is constantly cooled by the air in the lab as it rotates along the top half of the loop from point B to point A. When it reaches point A at time t_2, it has experienced the maximum amount of cooling that the air in the lab has to offer. As a result, it is the coolest pocket of fluid in the entire tube. Since these two antipodal pockets of water reach points A and B at the same time t_2, their difference in temperature is a direct indication of the direction of rotation of the fluid.

Conversely, if the fluid initially begins to rotate in a clockwise direction, the temperature at point A will always be greater than the temperature at point B by the same argument, and the fluid will continue to rotate in a clockwise direction. Clockwise rotation results in a measurement of δT = T_A - T_B greater than zero.

The work done by Creveling et.al. indicates that there is a distinct range of values for the heating rate V under which the thermosyphon remains in a stable state (CRV). In other words, for heating rates V within the range $V_i < V < V_{crit}$, the fluid in the tube rotates in only one direction from the moment conduction gives way to convection until the heat source is turned off. With the heat source set to supply any V in this range, the future behavior of the system is thus very predictable. If the transient behavior dies out at time t_i, and the system reaches a balance or equilibrium between the heating and cooling of the tube, we can accurately predict the direction of rotation with no uncertainty, as well as the temperature difference δT, from t_i to any later time t. The velocity of rotation and the temperature difference δT are virtually constant for any heating rate V within the stable range.

For heating rates within the stable range, weather forecasting in our thermosyphon is easy. Given the current state of the system, defined by V and δT, any future state of the system is unchanged once transient behavior dies out. However, this ability to predict the weather is lost once the heating rate is increased outside the stable range. For $V > V_{crit}$, the fluid never reaches a stable state. After the transient behavior dies out, the fluid will oscillate in a chaotic manner, changing from clockwise to counterclockwise rotation at irregular intervals. Any attempt to predict the future state of the system, δT, based on the current δT will result

in an exponential growth in uncertainty. This growth in uncertainty is common to all chaotic systems which exhibit the sensitive dependence on initial conditions that was discussed in Chapter 1. The chaotic behavior of the fluid in the thermosyphon illustrates complications that could very well occur when trying to forecast weather in the Earth's atmosphere. The same effects are thought to be responsible for the periodic inversions of the Earth's magnetic field, as well as the periodicity in the motion and size of sunspots, which are related to the sun's magnetic field.

Experimental Apparatus

The thermal convection loop for this experiment was constructed out of transparent plastic tubing with a melting point of 180 degrees Fahrenheit. The inner diameter, of the tube is 1 inch, with a wall thickness of $\frac{3}{16}$ of an inch. The loop is supported vertically in a circular shape of radius 13 inches. The fluid used to fill the tube, and model the air in the Earth's atmosphere, is water taken from the tap. Two holes were drilled in the joint connecting both ends of the tube, to allow for colored dye to be added to the water for visual analysis.

The top half of the tube is cooled by the room temperature air in the lab, $\approx 70^\circ$ F. The bottom half of the loop is heated by heating tape connected to a Variac which can produce temperatures between 70° and 450° F. Two lengths of heating tape are wound tightly around the tube in an attempt to create a constant and uniform heat source along its wall. The Variac allows for small adjustments in the amount of heat energy being transmitted to the water in the bottom half of the tube. The ability to accurately adjust the heating rate parameter is crucial to modeling chaotic behavior in the atmosphere. The temperature difference δT = T_A - T_B is measured a few times each second by a digital dual channel thermometer, and recorded manually every 15 seconds.

Observations

As mentioned before, past research on thermal convection loops predicts that there are there are two important values of the heating rate V: the rate at which conduction gives way to convection, V_i, and the rate at which stable convection gives way to unstable convection, V_{crit}. For our apparatus, the heating rate V corresponds directly to the power V the Variac supplies to the heating tape. The direct proportion relating V and V has been not been established, so to avoid confusion we will use V when referring to both the heating rate and the Variac power. In what follows, we characterize the power supplied by the Variac in terms of the settings on its adjustment dial, which are given in Volts.

Experimental trials show that $V_i \approx 5$ Volts for our thermosyphon. This means the water in the tube remains motionless for any trial with $V < 5$ Volts. Conductive behavior is observed numerically by the digital thermometer which reads $\delta T = 0$ even as the water in the tube heats up.

For heating rates above 5 Volts, the decrease in density of the warm pockets of fluid results in a buoyant force greater than the sum of the forces from gravity and viscosity, causing convection. Because of the geometry of the thermal convection loop, the fluid is forced to rotate rather than to simply rise and mix. Even though it can, in principle, be determined, we do not attempt to predict the direction in which the fluid will begin to rotate.

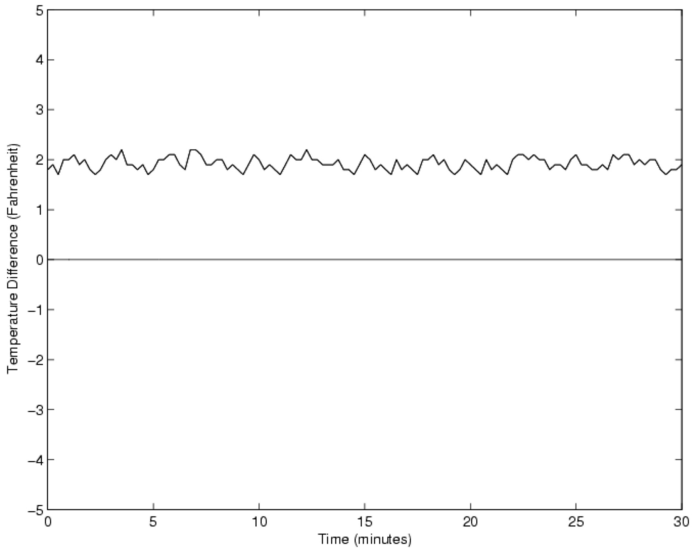

FIGURE 6. 20 Volts, 90° F at 6 o'clock

However, once the fluid has begun to rotate for some V in the range $V_i < V < V_{crit}$, it will maintain that direction of rotation "forever."

We now look at experimental results in the form of a graph of δT versus time. It is important to note that the initial time on the graph, $t = 0$ minutes, is not the time at which the Variac is turned on. For all of the experimental trials, the tube is given time to come to an overall average equilibrium temperature. If we took data immediately after the heating began, it would be difficult to reproduce. For small values of V, below 10 Volts, the time allotted for transient behavior to die out is around 2 hours. For values of $V > 10$ Volts, the tube needed up to 24 hours to achieve an equilibrium temperature.

A plot of δT verses time is shown in figure 6 for the heating rate corresponding to $V = 20$ Volts. The temperature difference is measured in degrees Fahrenheit, while time is plotted in minutes. The title of the plot states that the temperature at point C on the thermosyphon, or 6 o'clock on the face of the loop, was 90° F. This value is taken to be the average temperature of the bottom half of the loop, and corresponds to T_w in Chapter 2.

There are a few interesting facts that can be observed in this graph. First, $\delta T > 0$ for the duration of the experiment, which means that the fluid was always rotating in a clockwise direction. While data was only taken for 30 minutes, the stable nature of the system ensures that clockwise rotation would continue for as long as desired. Secondly, δT is relatively constant, oscillating slightly near 2° F. This means that the temperature T_A at point A is always about 2° warmer than T_B at point B. Since the fluid is incompressible, we can conclude that the velocity with which the fluid is rotating is very nearly constant as well. We can confirm this by injecting a spot of food coloring dye into the rotating water and timing its trip around the tube. Finally, and most importantly, we can predict the future state of the thermosyphon with very little uncertainty. That is to say, we know $\delta T \approx 2° \ \forall t$. The system is in a stable state and "weather forecasting" in our thermal convection loop is easy.

Figure 7 shows the results of an experimental trial with a heating rate of $V = 49$ Volts. At this rate, the temperature at point C is near 169° F. The graph looks very similar to the one shown previously for $V = 20$ Volts. The water in the tube is flowing in a clockwise direction with $\delta T \approx 2$ degrees. Once again, the future state of the thermosyphon, and thus

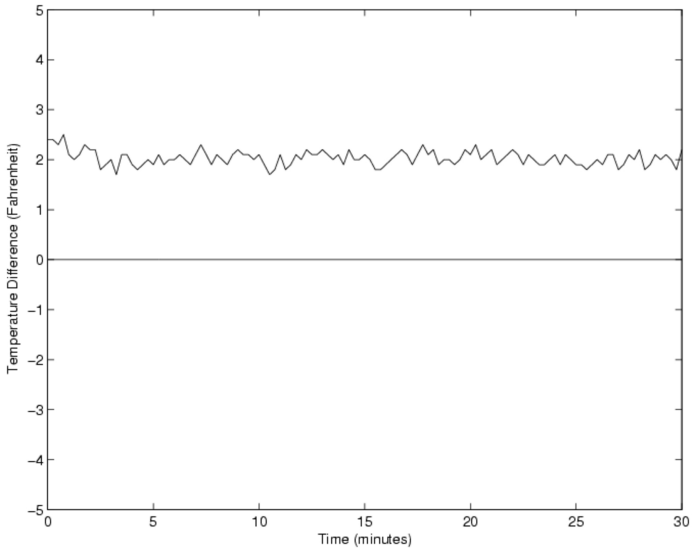

FIGURE 7. 49 Volts, 169° F at 6 o'clock

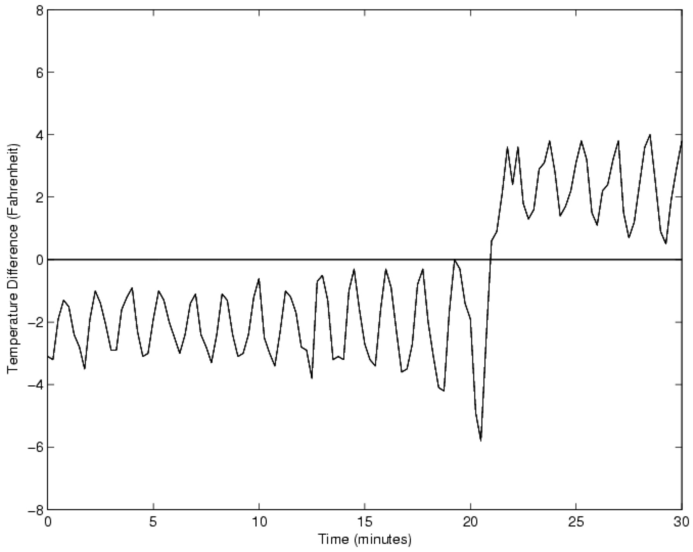

FIGURE 8. 50 Volts, 172° F at 6 o'clock

the future state of the "weather" in the tube, is very predictable. It should be noted here that for heating rates above $V = 49$ Volts, the heating tape is in danger of melting the plastic tube, since the melting point of the tube is 180° F. In hopes of finding the heating rate at which the system behaves chaotically, V_{crit}, one final trial was attempted with a heating rate of $V = 50$ Volts. Fortunately, the God that doesn't play dice has a sense of humor. The plot of δT verses time for this heating rate is shown in figure 8.

There are many interesting and important things to notice in the plot of δT for $V = 50$ Volts. First, increasing the heating rate V by one volt has increased the temperature at point C by only 3° F, from 169° to 172°. But this very small change in the heating rate, and consequently the overall average temperature, has turned a stable and predictable system into a chaotic and unpredictable one. We have found that $V_{crit} = 50$ Volts for our

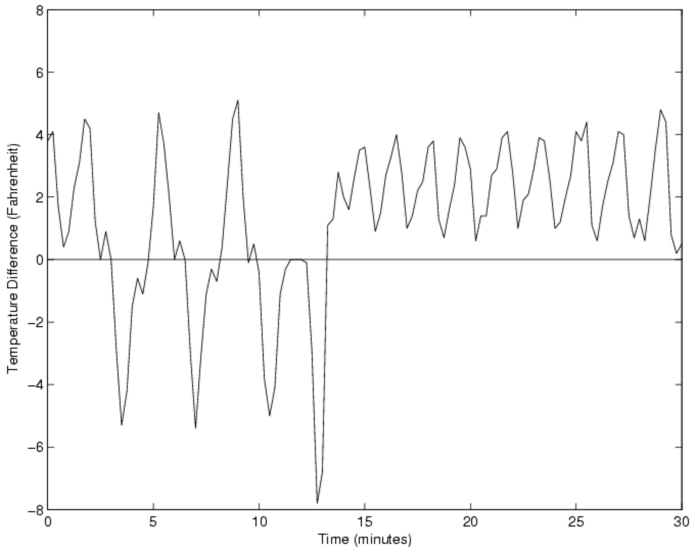

FIGURE 9. 50 Volts, 172° F at 6 o'clock

thermosyphon. Secondly, at the onset of the collection of data, the water in the tube is rotating in a counterclockwise direction, since $\delta T < 0$. Then 22.5 minutes later, the water spontaneously switches its direction of rotation, and begins to rotate in a clockwise manner. This result is surprising, considering how stable the system was when the heating rate was one volt less. It is also surprising considering the fact that the thermosyphon was allowed 24 hours to come to equilibrium before this data was taken. This result is very counterintuitive, but the reversal of flow was also observed visually when colored dye was dropped into the fluid at the joint in the open part of the tube.

Another intriguing aspect of the experiment illustrated by the plot is the oscillation in amplitude of δT. During the first 10 minutes of the trial, δT is oscillating around $\delta T = -2°$ F, between $-1°$ and $-3°$. This amplitude increases as time passes, to the point where δT is oscillating between $0°$ and $-4°$. Once this minimum value of δT is reached, the fluid switches its direction of rotation and begins to increase its amplitude of oscillation in a similar fashion as before. After $t = 22.5$ minutes, δT oscillates around $+2°$ F.

It is clear that the values of δT around which the temperature differences oscillate are $+2°$ and $-2°$. However, $+2°$ and $-2°$ are also the values of δT measured for experimental trials with $V < 50$ volts. This is unlikely to simply be a coincidence, but there is no theoretical prediction in any literature that predicts this will occur. The increase in oscillation amplitude is the one predictable behavior of the thermosyphon in a chaotic state. Further trials reveal that once the amplitude of δT reaches an absolute value above $\approx 4°$ F, the water in the tube switches its direction of rotation. Recent studies by Dr. Eugenia Kalnay at the University of Maryland indicate that the Lorenz state variables give a similar indication of the onset of a flow reversal.

The trial shown in figure 9 is a good illustration of the predictability of a switch in flow direction once a $|\delta T| > 4°$ F is reached. This trial was also done with a heating rate V corresponding to 50 Volts. In the first 15 minutes that data was taken, the water in the tube changed its direction of rotation 6 times! Then for the second half of the experiment, the water rotated in a clockwise direction, with δT constantly increasing its amplitude of oscillation. The spontaneous reversals of flow in the first half of the trial are not the result of perturbations or forces outside of those mentioned already. The behavior is simply chaotic.

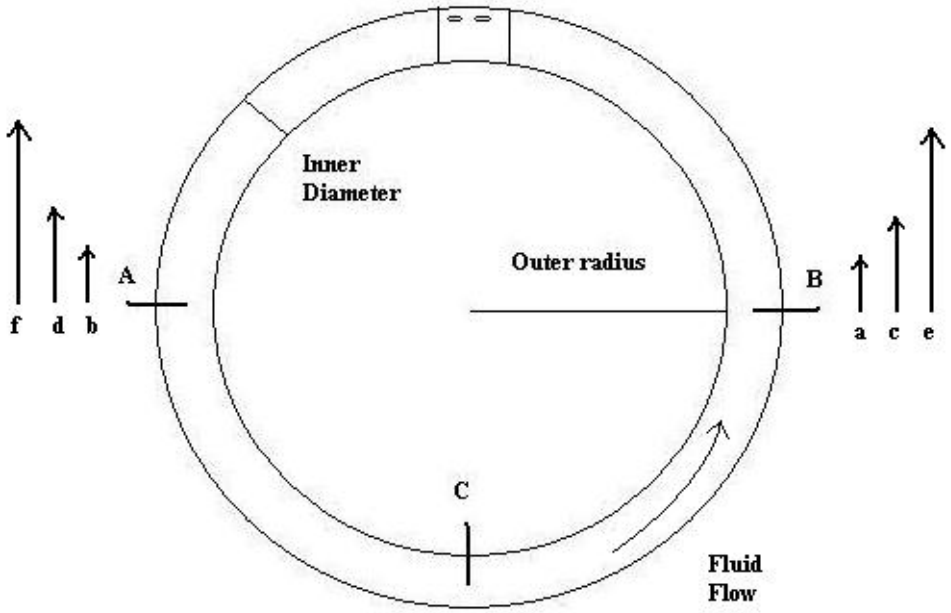

FIGURE 10. Anomoly generating flow reversal

It must be noted that the experimental results of Creveling indicate the existence of another important range in the heating rate V (CRV). For heating rates above some V_s, the fluid in the thermosyphon becomes stable again. That is to say, for $V > V_s$, the fluid in the tube behaves like it did for heating rates $V < V_{crit}$, rotating in one direction forever. Also, the direction of rotation remains stable until the heating tape nears the boiling point of the fluid. When the boiling point is near, the fluid becomes increasing turbulent and fails to model convection in the atmosphere. Unfortunately, due to the limitations of the plastic tubing we used to build our thermosyphon, V_s was never found since $V > V_{crit} = 50$ Volts melted the plastic and destroyed the apparatus!

Before we begin our discussion of how the Lorenz equations relate to the thermosyphon experiment, we present a physical explanation of the flow reversals. Assume the flow is counterclockwise and that an anomolous 'hot' pocket of fluid arrives at point B in the tube, figure 10. Due to some instability in the heating flux across the bottom half of the tube, this pocket is hotter than it should be. The hot pocket exerts a buoyancy force on the fluid, causing a positive acceleration in the counterclockwise direction and speeding up the rotation, arrow a. This pocket cools less on its journey across the top half of the tube, arriving at point A hotter than it should be. Consequently, there is a buoyancy force in the clockwise direction acting to slow down the speed of rotation, arrow b. The fluid decelerates, allowing the anomolous pocket more time to heat up as it passes point C. Upon arriving at point B, the pocket is once again hotter than it should be, by a greater amount now than before. The buoyancy force acting to accelerate the flowrate is greater this time since the instability has been magnified, arrow c. With even less time to cool off, the pocket crosses the top half of the tube to point A. The instability continues to grow, decelerating the clockwise flow again, arrow d, accelerating the flow, arrow e. This amplification will continue until the buoyancy force generated by the pocket at point A grows large enough, causing the flow to

stop. With no rotation in the tube, the temperature gradient between the top and bottom portions of the fluid grows unchecked. The fluid then reverses the direction of rotation, and the behavior observed in figures 8 and 9 continues indefinitely.

The magnification of thermal instabilities is only observed at values of the heating parameter above V_{crit}. We conclude that this is a bifurcation value of the system. For $V < V_{crit}$, we observe periodic rotation. For $V > V_{crit}$, we observe chaos. The periodic behavior found for $V < V_{crit}$ may be due to some natural dampening of low energy systems.

CHAPTER 4

The Lorenz Attractor

The state of the "weather" in our thermosyphon, for any pocket of fluid, is described by the pocket's position, temperature, and velocity. In other words, knowing these three variables at any particular time is all that is needed to know them at any future time, and hence to forecast the state of the system at any future time. Unfortunately, we were unable to measure the velocity of the fluid in our thermosyphon. We were only able to measure the temperature difference between the warm rising fluid and the cool falling fluid on opposite sides of the tube. However, a technique known as *state reconstruction* can be used to uncover more information about the shape of the Lorenz-like attractor which corresponds to the behavior of the fluid in our thermosyphon.

State Reconstruction

Given a time series (a plot of a system measurement versus time), state reconstruction allows us to recover information about the system which we were unable to measure directly (ALL, 538). To see how, first recall that the temperature difference between the warm rising fluid and the cool falling fluid in a convection cell can be modeled using the function $Y(t)$ defined in Equation (41), Chapter 2. No explicit solutions for the function $Y(t)$ have been found, but numerical solutions to the Lorenz equations reveal the qualitative similarities between the behavior of $Y(t)$ and that of the fluid in the thermosyphon.

For a certain initial condition, figure 11 shows the time series of the function $Y(t)$ whose derivative is determined by the Lorenz equations. Compare this plot to that of the temperature difference measured experimentally with the thermosyphon for a heating rate of 50 Volts in figures 8 and 9. Much of the qualitative behavior of the function $Y(t)$ agrees with the experimental results, most notably the increase in oscillation amplitude prior to a reversal of flow. As a way to see how well the Lorenz equations describe the behavior of the fluid in our thermosyphon, we reconstruct the Lorenz attractor from the time series described in Chapter 3. To do this, we plot each measurement of the time series of temperature difference, δT (defined in Chapter 3), versus a time-delayed version. That is, given the measured value of δT at a time t, we find δT at a time $(t - \tau)$ where τ is called the delay. This allows us to determine whether δT is increasing or decreasing at time t.

We then plot $\delta T(t)$ versus $\delta T(t - \tau)$ and create a delay portrait for the temperature difference in the rotating fluid. If the behavior of the fluid were periodic, then the delay plot would appear as a closed loop in phase space. Since we know the behavior of the rotating fluid is not periodic for the thermosyphon, we don't expect the delay plot to be a closed loop. The choice of τ is crucial to being able to construct an accurate delay plot. If τ is too small, the behavior of δT won't have had time to change significantly from time $(t - \tau)$ to time t. As a result, the delay plot would appear almost like a plot of $y = x$, because $\delta T(t - \tau) \approx \delta T(t)$. If τ is chosen too large, then much of the important behavior of the function $\delta T(t)$ might be missed. For example, if the data we are attempting to create a delay plot for has many local maxima and minima, as our data does, a large τ might result in $\delta T(t -$

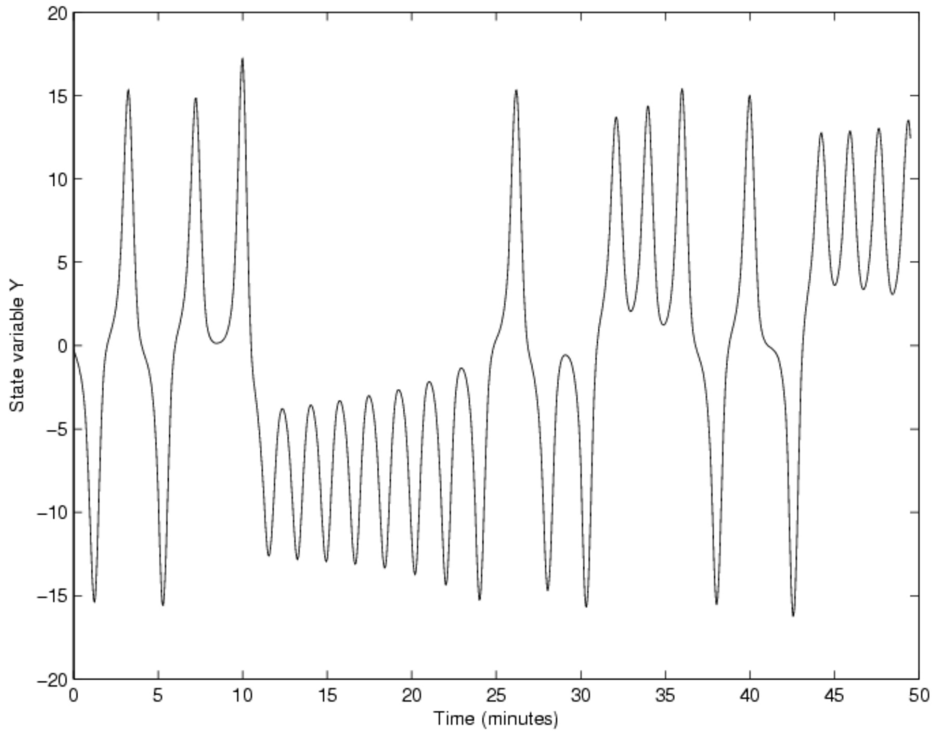

FIGURE 11. State variable Y, time series plot

$\tau) \approx \delta T(t)$ even when a peak or valley has occured at some time between (t - τ) and t. The peak or valley would be ignored in the delay plot because τ was too large.

The delay portrait we create by plotting $\delta T(t)$ versus $\delta T(t$ - $\tau)$ can also be ambiguous when the two functions map to the same point in phase space at two or more different times. If we follow a trajectory through the phase space created by the delay plot by allowing time to pass, and we reach an intersection in the trajectory, we will be unable to determine the direction in which to travel. To attempt to resolve the difficulty, we add a third dimension to our delay plot. If there are no self-intersections in three space, the implication is that knowing the three values at any time t would be enough to say what happens next. In such a case, there would only be one direction to travel along the trajectory at any point in time. For the Lorenz equations, the third dimension in our phase space is recovered by creating a third function, $\delta T(t$ - $2\tau)$. If we then plot the three functions together, [$\delta T(t)$, $\delta T(t$ - $\tau)$, $\delta T(t$ - $2\tau)$], we create an approximation of the Lorenz attractor (ALL, 547).

We now reconstruct the two dimensional Lorenz attractor from our thermosyphon measurements of δT, taking $\tau = 15$ seconds to be the time delay. This τ is necessarily large because data was only taken every 15 seconds. Figure 12 plots the measurements of δT taken over the course of an hour. The two-dimensional delay reconstructed attractor for our data is shown in figure 13. In this reconstructed phase plot, points are plotted every 15 seconds and joined by straight line segments to make their progression easier to follow.

Consider now, plotting δT versus $\delta T(t$ - 15s) versus $\delta T(t$ - 30s) in three space. This will give us a three dimensional phase portrait of the behavior of the fluid in our thermosyphon, figure 14. Note how the three dimensional plot appears to have a shape similar to that of the Lorenz attractor. While the nature of the attractor is far more apparent when viewed as the picture is created, the state reconstruction is successful in recovering the Lorenz attractor for our thermosyphon data. In particular, there don't appear to be any self intersections. In

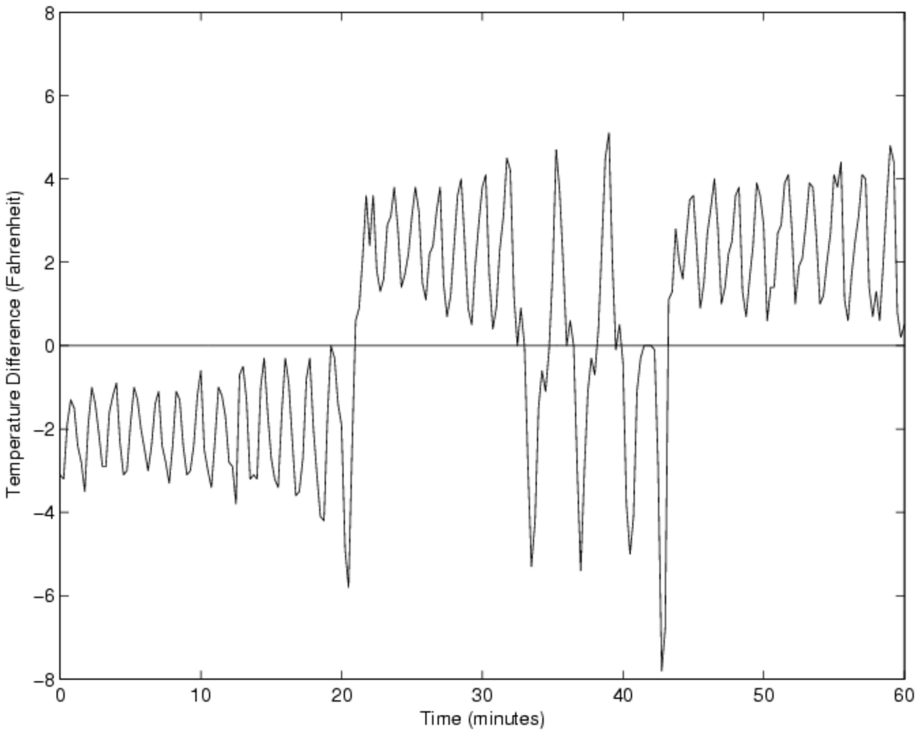

FIGURE 12. Raw Delta T data

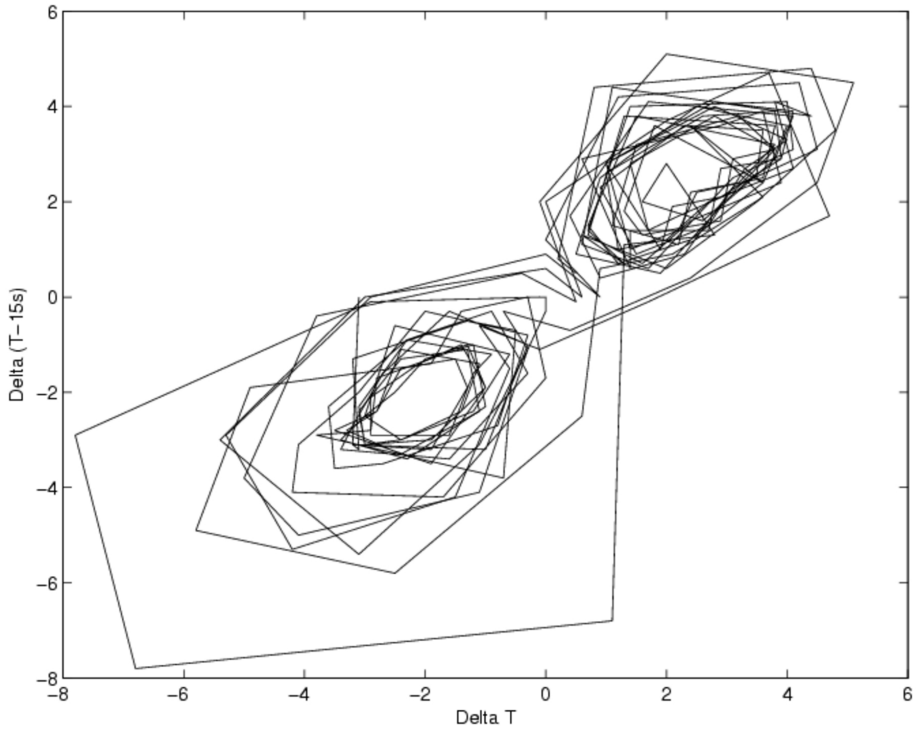

FIGURE 13. Two-dimensional delay reconstruction

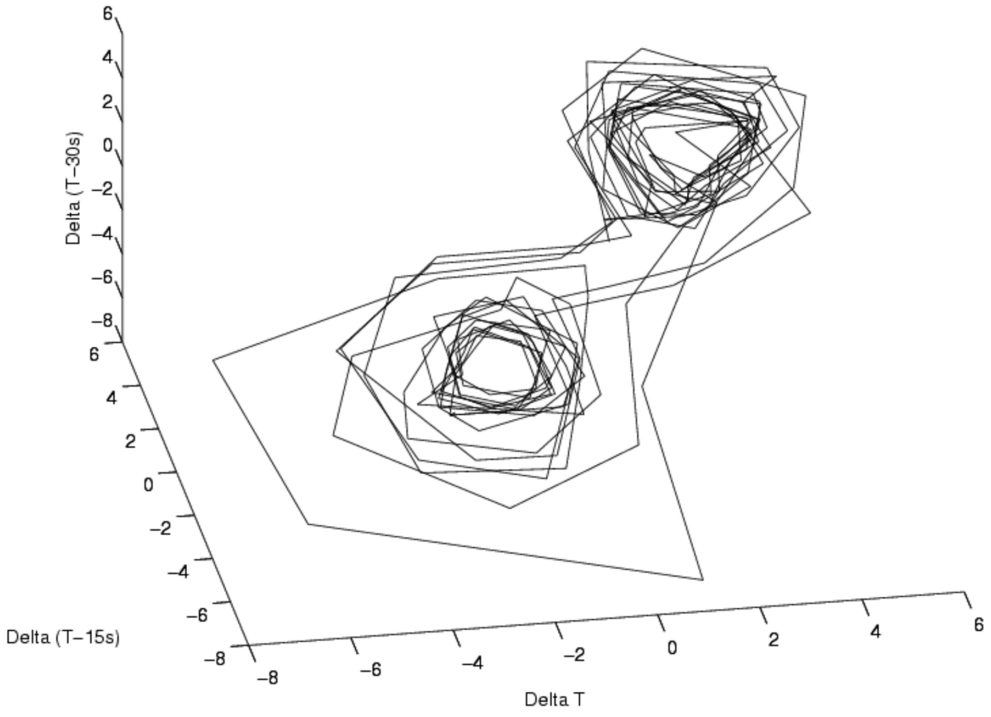

FIGURE 14. Three-dimensional delay reconstruction

other words, no single data point seems to have four line segments meeting at it, indicating that knowing δT, $\delta T(t$ - 15s), and $\delta T(t$ - 30s) exactly at any time t allows for prediction of future states.

Cubic Splines and a Smooth Attractor

The temperature difference data δT was only taken every 15 seconds. As a result, the reconstructed attractor for our thermosyphon has a number of jagged edges. To remedy this, we smooth the data in our time series plot of δT, and examine the consequences of this smoothing on the state reconstruction plots.

While our data was only taken every 15 seconds, the actual behavior of δT was changing continuously. Plots of data collected more frequently would produce smoother curves. For the collection of 15-second time intervals between data points, we use a technique known as *cubic spline interpolation* to find cubic polynomials that have the same values as our data over each time interval, and use them to smoothly connect each consecutive pair of data points with the proper inflection (KIN, 317). In a sense, the cubic spline fills in or interpolates the values of δT which we would have otherwise measured directly. For our 242 data points, we find 241 separate cubic splines to draw a smooth graph. Fortunately, computers can be programmed to find the necessary cubic polynomials so we don't need to find all 241 by hand! The resulting time series of δT, smoothed using cubic spline interpolation, is shown in figure 15. Only a segment of the data is shown, with the raw data shifted 2 units up.

With this smoother time series, we again reconstruct the Lorenz attractor for our thermosyphon. Since the cubic spline allows us to pretend we have continuous data, we can choose a more appropriate value for the time delay τ. For the shape of the time series, we

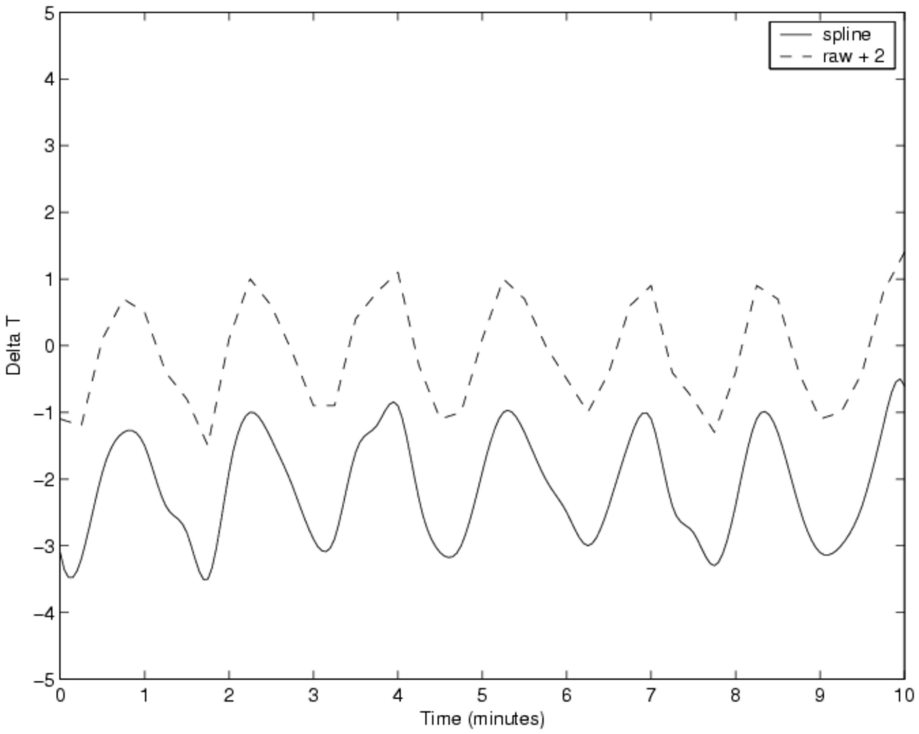

FIGURE 15. Segment of smoothed data

choose a value of $\tau = 1.5$ seconds, one-tenth of our original value. We tried smaller values of τ and as expected they resulted in delay plots very close to the line $x = y = z$.

Now that our time series looks more like numerical approximations of $Y(t)$, we plot the three functions $\delta T(t)$, $\delta T(t - \tau)$, and $\delta T(t - 2\tau)$. The resulting "smoothed" and reconstructed attractor for our thermosyphon data is shown in figure 16. Here we are using a delay of 3 seconds, compare with figure 14 which used raw data and a delay of 15 seconds.
Notice how the attractor in figure 16 appears to be "thinner" than that in figure 14, created without the help of cubic spline interpolation. This is a drawback to state reconstruction, due to the sensitivity in the choice of τ. As mentioned before, if τ is small, the values of $\delta T(t)$, $\delta T(t - \tau)$, and $\delta T(t - 2\tau)$ will be very close, resulting in a curve lying very close to the line $x = y = z$. This makes the absence of self-intersections less clear, which is unfortunate, since a lack of self-intersections is what we need in order to know that values for $\delta T(t)$, $\delta T(t - \tau)$, and $\delta T(t - 2\tau)$ are enough to determine any future state.

Ross Reconstruction

In an attempt to resolve the problems created by the time delay τ in delay plot reconstruction, we develop a new way to reconstruct the Lorenz attractor. Rather than plotting data points as a function of previous data points, we plot data points versus the rates of change of the function in question at the same time. In other words, to reconstruct the Lorenz attractor for our function $Y(t)$ from Chapter 2, we plot $Y(t)$ vs. $Y'(t)$. In this method, the dT we choose for our numerical approximation of $Y(t)$ is analogous to τ, but we are free to choose an arbitrarily small dT without collapsing our reconstructed attractor down onto the line $x = y = z$. Greater flexibility in the time step dT is the main advantage

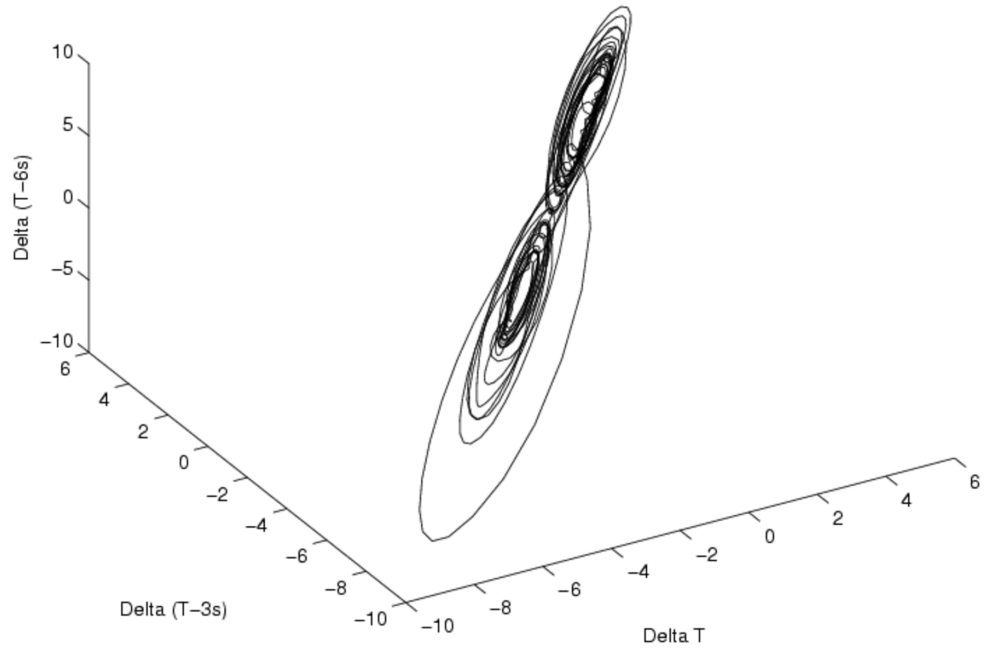

FIGURE 16. Three dimensional smooth delay reconstruction

of Ross reconstruction. An example of Ross reconstruction is shown in figure 17 for the function $Y(t)$ from Chapter 2. The reconstruction was made with a time delay of 0.01. The Ross technique is then applied to the smoothed thermosyphon data by plotting approximations of $\delta T(t)$ vs. $\delta T'(t)$, shown in figure 18 for $\tau = 0.001$ seconds.

This figure appears to be very similar to the actual Lorenz attractor, and most importantly, it is easier to see that there are no self-intersections in the phase trajectory. It is very easy to believe in the lack of intersections when the plot is viewed as it is drawn by the computer in real time. Trajectories spiral outward from one focus until a critical distance is reached, at which point they dive in towards the other focus. Any trajectory for this system will follow this pattern forever, without ever intersecting itself.

The approximations for the three functions $\delta T(t)$, $\delta T'(t)$, and $\delta T''(t)$ are made using the cubic spline interpolated data for $\delta T(t)$. The formulas used for $\delta T'(t)$ and $\delta T''(t)$ allow for an arbitrarily small time step, and are shown in equation (44).

$$\delta T'(t) = \frac{\delta T(t) - \delta T(t - \tau)}{\tau} \text{ and } \delta T''(t) = \frac{\delta T(t) - 2\delta T(t - \tau) + \delta T(t - 2\tau)}{\tau^2}. \tag{44}$$

Success! The reconstructed attractor looks more like the Lorenz attractor than that generated using delay plot reconstruction. In a manner similar to the Ross reconstruction of $Y(t)$ shown in figure 17, this trajectory spirals out around the right hand side of the attractor before looping around to the left hand side. As the computer draws this picture, it is easy to see that there are no self-intersections. The Ross method of data reconstruction has been used to uncover the Lorenz attractor associated with our thermosyphon data!

Conclusions

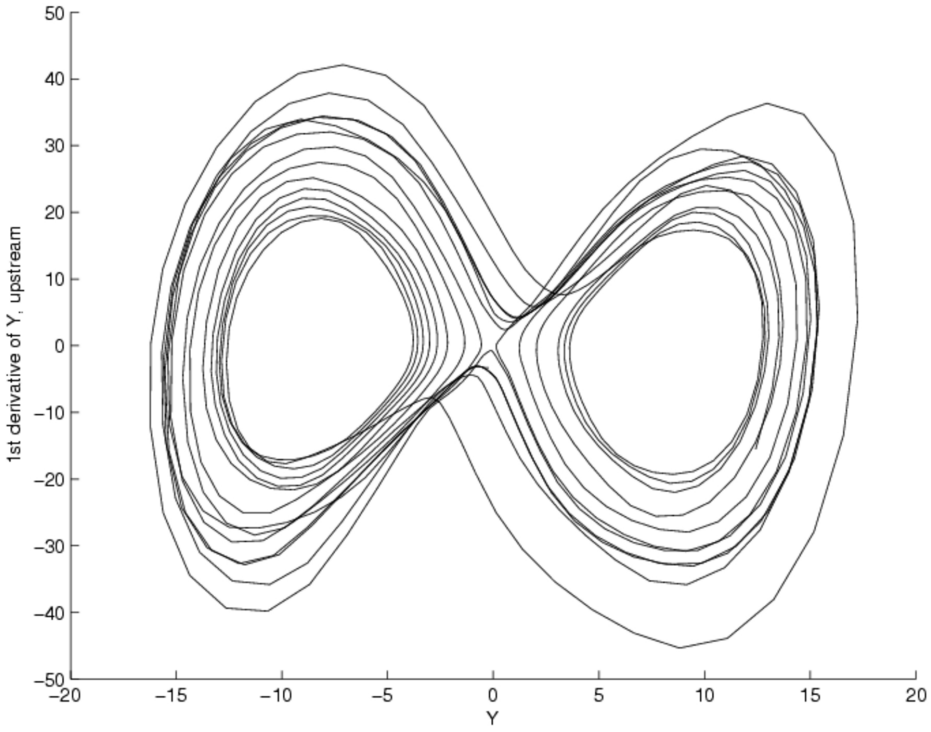

FIGURE 17. Reconstructed Lorenz attractor for figure 11

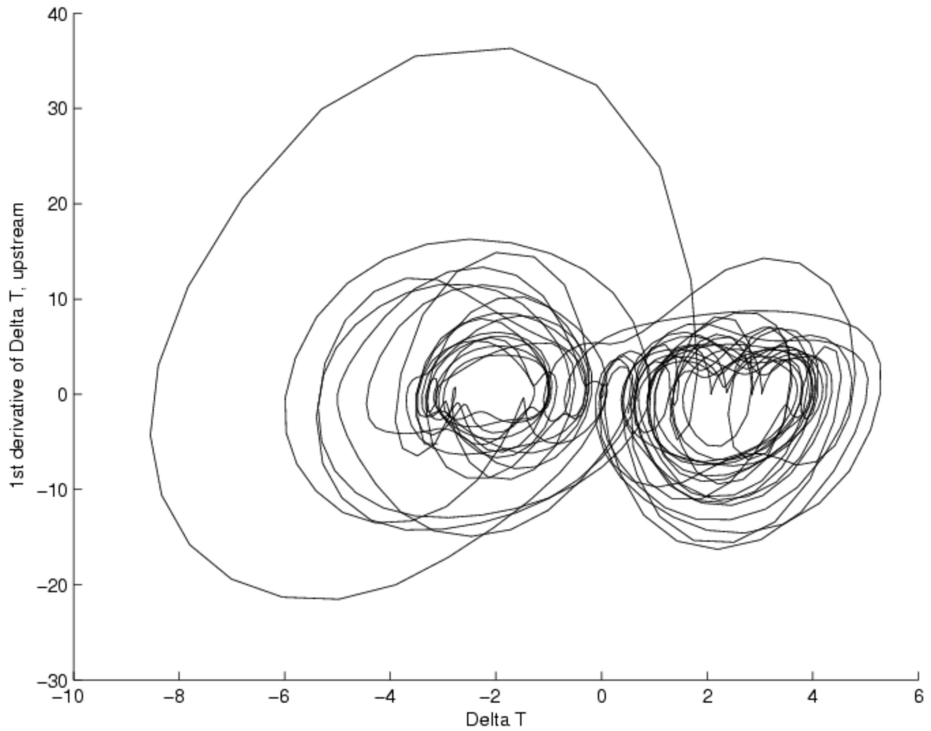

FIGURE 18. Ross reconstruction of attractor for smoothed experimental data

In order to demonstrate some of the difficulties associated with weather prediction, we derived a set of differential equations which model convection in the atmosphere. We then built a convection experiment known to illustrate the chaotic behavior of a rotating fluid. To compare data taken from our thermosyphon with predictions made by the Lorenz equations, we successfully used data reconstruction techniques to reproduce the Lorenz attractor. In the future, measurements of the velocity of the fluid in the thermosyphon could be compared to the function $X(t)$, and then used to reconstruct a more accurate attractor.

Bibliography

[ALL] K. Alligood, T. Sauer, and J. Yorke, *Chaos: An Introduction to Dynamical Systems*, Springer, New York, 1996.

[BUR] William Burroughs, *The Climate Revealed*, Cambridge University Press, New York, 1999.

[CHN] S. Chandrasekhar, *Hydrodynamic and Hydromagnetic Stability*, Dover Publications Inc., New York, 1961.

[CRV] H. F. Creveling, J. F. De Paz, J. Y. Baladi, and R. J. Schoenhals, *Stability Characteristics of a Single-phase Free Convection Loop*, Journal of Fluid Mechanics, **67** (1975), 65-84.

[GLK] James Gleick, *Chaos*, Viking, Canada, 1987.

[GSN] J. P. Gollub and Harry Swinney, *Onset of Turbulence in a Rotating Fluid*, Physical Review Letters, **35** (1975), 927-930.

[HLB] Robert Hilborn, *Chaos and Nonlinear Dynamics*, Oxford University Press, Oxford, 1994.

[KIN] David Kincaid and Ward Cheney, *Numerical Analysis*, Brooks/Cole Publishing Company, California, 1991.

[LOR1] Edward Lorenz, *Deterministic Nonperiodic Flow*, Journal of the Atmospheric Sciences, **20** (1963), 130–141.

[LOR2] Edward Lorenz, *The Circulation of the Atmosphere*, American Scientist, **54** (1966), 402–420.

[LOR3] Edward Lorenz, *The Essence of Chaos*, University of Washington Press, Seattle, 1993.

[OTT] Edward Ott, Tim Sauer, James A. Yorke, *Coping With Chaos*, John Wiley + Sons Inc., New York, 1994.

[PAT] A. R. Paterson, *A First Course in Fluid Dynamics*, University of Cambridge Press, Cambridge, 1983.

[SLZ] Barry Saltzman, *Finite Amplitude Free Convection as an Initial Value Problem*, Journal of the Atmospheric Sciences, **19** (1962), 329–341.